Bioprinting 18 (2020) e00083

Contents lists available at ScienceDirect

Bioprinting

journal homepage: www.elsevier.com/locate/bprint

Novel bioinks from UV-responsive norbornene-functionalized carboxymethyl cellulose macromers

Shen Ji [a], Alperen Abaci [a], Tessali Morrison [b], William M. Gramlich [b], Murat Guvendiren [a,c,*]

[a] Otto H. York Chemical and Materials Engineering, New Jersey Institute of Technology, 161 Warren Street, 150 Tiernan Hall, Newark, NJ, 07102, USA
[b] Department of Chemistry, University of Maine, 156 Aubert Hall, Orono, ME, 04469, USA
[c] Department of Biomedical Engineering, New Jersey Institute of Technology, USA

ARTICLE INFO

Keywords:
Cellulose
Click-chemistry
Additive manufacturing
Bioprinting
Stem cell
Hydrogel

ABSTRACT

3D printing has significantly progressed in the past decade and become a potentially powerful biomanufacturing approach for tissue and organ printing. Availability of diverse hydrogel-based bioink formulations, particularly bioinks allowing biochemical functionalization, stimuli responsiveness, and control over mechanical and degradation properties are crucial for bioprinting to reach its full potential. In this study, we report two novel bioink platforms from norbornene modified cellulose-based macromers, either with an amide, norbornene CMC (NorCMC), or an ester linker, carbic (norbornene) functionalized CMC (cCMC). Both of the bioink formulations show autogelation in the absence of UV light, which allow us to adjust the viscosity of the ink formulation. Bioinks rapidly form cell-laden hydrogels when exposed to UV light due to photoinduced thiol-ene crosslinking mechanism. Bioink viscosity and printability as well as bioprinted construct mechanics are controlled by bioink concentration and thiol to norbornene (T:NB) ratio. Human mesenchymal stem cells (hMSCs), NIH 3T3 fibroblasts, and human umbilical vein endothelial cells (HUVECs) are successfully bioprinted using our novel bioink formulations. Considering the high abundance, low cost, ability to selectively tether molecules or control crosslinking properties, norbornene modified cellulose-based bioink platforms have a significant potential to enable 3D bioprinted constructs with increased complexity.

1. Introduction

Three-dimensional (3D) bioprinting is an emerging field with a significant potential to create custom-designed and patient-specific "living" constructs using a patient's own medical images and cells [1–4]. 3D bioprinting could potentially eliminate organ shortage [5–8] and enable development of patient-specific tissue models for personalized drug screening [9–13]. A recent frontier is in situ bioprinting for reparative or regenerative therapy, in which a living tissue is printed directly at the site of an injury or a defect [14–16]. Despite the strong potential of bioprinting and recent advancements in the bioprinting technology, there is a notable lack of diversity in bioinks which significantly hinders the widespread use of bioprinting.

3D bioprinting enables layer-by-layer manufacturing of a living construct from bioinks, which are bioprintable formulations composed of cells that are usually supported with a hydrogel [17]. The requirement for live cell printing significantly limits the number of additive manufacturing technologies that are suitable for bioprinting [18]. Bioprinting technologies include extrusion-based direct ink writing (DIW), droplet-based inkjet printing, and light-based approaches, including projection stereolithography and laser-induced forward transfer (LIFT) [18–20]. DIW is the most commonly used technique due to its availability, affordability, and ease of use. In DIW, a bioink formulation is extruded through a blunt needle to form a self-supporting structure. In this process, the bioink should meet the basic requirements for extrusion-based bioprinting [21–23], such that it should *(i)* have a suitable viscosity, i.e., low enough for easy extrusion yet high enough for formation of self-supporting layers post-printing to minimize sagging, usually in the range of 30 to 6 $\times$ 10^7 mPa s, and *(ii)* allow printing of living cells and support high viability (>90%) [17,21,22]. In addition, the bioink and its degradation products should be cytocompatible and should not induce an inflammatory response when implanted [22,24].

Most commonly used bioinks are formulated from cell-laden hydrogels due to their high water content and properties mimicking native

* Corresponding author. Otto H. York Department of Chemical and Materials Engineering, New Jersey Institute of Technology, 161 Warren Street, 150 Tiernan Hall, Newark, NJ, 07102, USA.
E-mail address: muratg@njit.edu (M. Guvendiren).

https://doi.org/10.1016/j.bprint.2020.e00083
Received 19 September 2019; Received in revised form 24 January 2020; Accepted 4 March 2020
2405-8866/© 2020 Elsevier B.V. All rights reserved.

tissue microenvironment [25,26]. A variety of hydrogel-based bioinks have been developed from synthetic (such as Pluronic [27,28] and poly(ethylene glycol) [29]), or natural (gelatin [30–32], hyaluronic acid [33,34], alginate [33,35], chitosan [36], collagen [37,38], fibrin [39], and silk [40,41]) polymers/macromers, or decellularized tissue materials (e.g., heart, bone, liver, pancreas, etc.) [42,43]. The building blocks of these formulations are usually modified to allow tunable viscosity and shape fidelity during printing process. Although innovative approaches have been developed to control printability including pre-crosslinking to control flow [29] or rapid crosslinking during or after-printing [44,45], or designing shear thinning formulations [34,46], novel bioink formulations are still needed to broaden the currently available bioink "library" and to develop stimuli responsive bioinks enabling control of bioprinted construct properties post-printing.

In this study, we focused on carboxymethyl cellulose (CMC), a commonly used cellulose derivative. Cellulose is one of the most abundant and renewable natural polymers [47,48]. As a natural polymer, cellulose is inherently bioactive, biodegradable, and biocompatible [47]. The hydroxyl groups on its backbone structure allows functionalization of cellulose to tune its properties [49]. When compared to cellulose, CMC is highly soluble in water due to its carboxyl groups [50] making it an attractive building block for hydrogels. CMC-based hydrogels have been developed utilizing a wide range of crosslink mechanisms including physical and chemical crosslinking [13]. For instance, Nie et al. reported CMC-based hydrogels by crosslinking sodium CMC with $AlCl_3$, and studied the effects of crosslinker, CMC concentration and temperature on hydrogel stiffness and degradation [16]. Chemically crosslinked CMC-based hydrogels have been developed using irradiation-initiated [17–19], photo-initiated radical [20,21], enzymatic [22], and epoxide-opening reactions [23]. For instance, methacrylated CMC is synthesized to allow photo-initiated radical reaction to fabricate CMC-based hydrogels. These hydrogels were used to facilitate chondrogenic differentiation of encapsulated human mesenchymal stem cells (hMSCs) encapsulated within the hydrogels [21].

Cellulose has been used as a filler, or as a component, in ink formulations [51–54]. Majority of the studies focused on cellulose/alginate based ink formulations, utilizing a range of cellulose derivatives (nanofibrillated cellulose, nanocellulose, and methylcellulose) and taking advantage of physical crosslinking ability of alginate with $CaCl_2$ [55–60]. For instance, nanocellulose-alginate based bioinks were developed for 3D bioprinting of human chondrocyte-laden hydrogels for cartilage regeneration [55,61]. Muller et al. developed alginate sulfate/nanocellulose bioinks but reported significantly compromised proliferation ability of chondrocytes during printing process [58]. Markstedt et al. developed bioinks from cellulose nanofibrils mixed with xylan for crosslinking [62]. Most recently, methylcellulose (MC)-based hydrogels were printed utilizing the sol-gel transition, or lower critical solution temperature (LCST), allowing printing of MC-based hydrogels at 21 °C with high cell survival (80%) post-printing [63]. Li et al. developed highly thixotropic inks from alginate/methylcellulose blend hydrogels, and showed that the treatment of the printed constructs with trisodium citrate (TSC) significantly enhanced the interfacial bonding between printed layers [64]. Finally, Lewis group developed hydrogel composite inks composed of soft acrylamide matrix supported with cellulose fibrils, and crosslinked with clay [51]. They were able to selectively align cellulose nanofibrils during the printing process to develop 3d printed structures with anisotropic stiffness, which led to shape change on immersion in water. In this study, we develop novel photocurable bioink formulations directly from carboxymethyl cellulose (CMC) eliminating the need for alginate or other additives/components.

Light-induced free radical polymerization of methacrylates or acrylates is a widely used approach in designing photoreactive bioinks, yet this reaction is not specific and leads to formation of a heterogenous network composed of kinetic chains. Thiol-norbornene photo-click chemistry is specific to norbornene and thiyl radicals (i.e., radicals from thiols) as compared to norbornene radicals (its own radicals) or nonradical thiols [65,66]. This is important to achieve selectivity in crosslinking (crosslinkers containing multi-thiols) and tethering of biomolecules (containing mono-thiols). This mechanism ensures a more homogeneous crosslinking in a controllable manner [65,67,68]. Natural (such as alginate [69], hyaluronic acid [68,70], and gelatin [71,72]) and synthetic polymers (such as poly(ethylene glycol) [67,72,73]) have been modified with norbornene group to fabricate photocurable, cell-laden hydrogels. Recently, CMC has been modified with norbornene groups [50,74] to develop renewable hydrogels. Gramlich group recently demonstrated high cell viability of encapsulated stem cells within norbornene functionalized CMC [75]. Motivated by these recent results, we focused on developing novel bioink formulations from norbornene functionalized CMC.

In this study, we report two novel stimuli responsive bioink platforms from CMC for extrusion based bioprinting. CMC is functionalized with thiol-ene reactive norbornene (Nor) with an amide, norbornene CMC (NorCMC), or an ester linker, carbic (norbornene) functionalized CMC (cCMC). CMC was chosen as the building block for both of our bioink platforms due to its high availability and low cost, and high solubility in water. Light-induced thiol-ene click chemistry enabling norbornene was selected as the functional group to achieve selective crosslinking and selective tethering of biomolecules. Printability of the bioink platforms was determined by the thiol-Nor ratio for each macromer concentration. CMC-based bioink platform allows tunable printability, stiffness and high viability of bioprinted cells, and broadens the range of currently available bioink platforms.

2. Materials and methods

2.1. Polymer synthesis

The macromers, cCMC and NorCMC, were synthesized according to methods developed previously for cCMC [74] and NorCMC [75]. To synthesize cCMC, CMC (90KDa, 0.7 carboxymethyl groups per anhydroglucose unit, Sigma) was dissolved in reverse osmosis (RO) water at 1% (w/v). Then, 7.26 g of cis-endo-5-norbornene-2,3-dicarboxylic anhydride (carbic anhydride, TCI) was added to the CMC solution (per gram of CMC). The reaction was maintained for 2 h while the pH of the reaction was adjusted at the range of 9.0–10.5 by dropwise adding 10M NaOH. Subsequently, 10-fold volume of the reaction solution of ice-cold acetone was used to precipitate the reaction solution. The precipitate was collected by suction filtration and dissolved in RO water at 1% (w/v) and dialyzed (6–8 kDa) against RO water for 3 days followed by lyophilization. For NorCMC, sodium CMC (90KDa, Sigma) was dissolved in RO water at 1% (w/v), and 0.592 g of 1-ethyl-3-(3-dimethylaminopropyl) carbodiimide hydrochloride (EDC HCl), 0.356 g of N-hydroxysuccinamide (NHS), and 0.4 mL of 5-norbornene- 2-ethylamine (NA) were added (per gram of sodium CMC). The reaction solution was stirred and maintained at room temperature for 18 h. NaCl was added to the reaction solution, stirred at room temperature for 30 min, and the reaction solution was precipitated in 10-fold ice-cold acetone. The precipitate was dissolved in RO water at 1% (w/v) and dialyzed (6–8 kDa) against RO water for 3 days followed by lyophilization. The extent of the modification for both polymers was characterized using ^{1}H NMR spectroscopy using a Bruker Avance Neo 500 MHz spectrometer (NorCMC) and a Varian Inova 400 MHz spectrometer (cCMC).

2.2. Cell culture and maintenance

Human mesenchymal stem cells (hMSCs, passage 4, Lonza) were cultured in the growth media (MEM-α (Gibco), supplemented with 10% fetal bovine serum (FBS, Gibco) and 1% penicillin-streptomycin (pen-strep, Gibco)) at 37 °C and 5% CO_2. Growth media was refreshed every 3 days. Human umbilical vein endothelial cells (HUVECs, passage 5, Lonza) were cultured in EGM-2 media (EGM-2 Bullet Kit, Lonza). Media was changed every two days to ensure a proper cell proliferation. NIH 3T3 fibroblasts were cultured in DMEM (Gibco) supplemented with 10% FBS (Gibco) and 1% pen-strep (Gibco). Media was refreshed every 3 days.

2.3. Ink preparation

Ink formulations contained norbornene modified CMC (15% (w/v) for cCMC and 10% (w/v) for NorCMC) and 0.05% (w/v) lithium phenyl-2,4,6-trimethylbenzoylphosphinate (LAP, Allevi) in growth media. For instance, to prepare a 10% NorCMC, 100 mg of NorCMC was dissolved in 1 ml of 0.05% LAP stock solution in growth media in a glass vial, covered with an aluminum foil. The solution was stirred overnight at room temperature. To adjust the pH of the cCMC solution to pH = 7.5, 20 μl of triethylamine (Sigma Aldrich) was added to the cCMC solution.

To prepare a bioink, 900 μl of LAP stock solution was used to dissolve the polymer. Then, the solution was mixed with 100 μl of cell suspension (hMSC, 3T3, or HUVEC; 1×10^7 cells/mL) using a magnetic stirrer, leading to a final ink concentration of 15% cCMC (or 10% NorCMC). Each ink formulation was transferred into a BD Luer-Lok™ 10-mL syringe prior to printing. Prior to printing process, pre-calculated amount of the crosslinker (DL-dithiothreitol (DTT), Sigma) was added to the bioink formulation and stirred gently for 1 min.

2.4. Rheological characterization of the ink formulations

Malvern Ultra + Rheometer (flat plate geometry, 20 mm, 1 mm gap) was used to analyze the rheological properties of the ink formulations. To investigate the crosslinking process in the absence of light exposure, time sweep tests were performed at a frequency of 1 Hz and an oscillatory strain of 0.05%. Elastic modulus (G'), viscous modulus (G''), viscosity (γ) and phase angle (φ) values were recorded. To investigate the photo-crosslinking process, inks were casted on to the lower plate of the rheometer, and time sweep tests were performed using an optical kit (Malvern) connected to a UV light source (Omnicure S2000, 356 nm, 5 mW/cm^2). Light intensity was adjusted to represent the intensity during printing process (405 nm, 40 mW/cm^2) according to the molar absorptivity spectrum of the photoinitiator (LAP) [76]. The UV light was turned on for 4 min after 1 min of equilibrium time during time sweep tests. Initial viscosity values refer to mean of the viscosity values measured for the first 1 min prior to UV exposure.

2.5. Mechanical properties of the crosslinked ink formulations

Malvern Ultra + Rheometer (flat plate geometry, 8 mm) was used to measure the compressive modulus (Young's modulus, E) of the samples. Two sets of disc-shaped hydrogel samples (1 mm in thickness and ~25 mm in diameter) were prepared via direct casting followed by UV exposure and bioprinting process. Samples were kept in DPBS for 24 h to ensure equilibrium swelling. The compression test was performed by applying a compressive normal force to the hydrogel sample using the upper flat plate geometry while monitoring the gap distance (where strain is equal to the gap - sample thickness). To ensure initial contact, an initial compressive force equal to 0.05 N was applied. The compressive force was increased continuously (0.1 mm/s) up to 2 N. The compressive modulus (E) was obtained by calculating the slope of stress-strain curve (using the linear range within 10% strain).

2.6. Scaffold design

3D scaffold designs were created by Autodesk® Fusion 360™ and the 3D models were sliced with Slic3r in Repetier-Host to generate G-code files. A 15 mm × 15 mm grid-like 2-layer scaffold and a 12 mm × 8 mm 3-layer cuboid were designed for printability tests and cell viability tests.

2.7. Line test

Ink formulations were used to print individual struts (lines) on a glass slide at different print pressures and speeds. The images of the printed struts were captured by a microscope. Three random parts of each strut (from three samples per each group) were captured for analysis. The strut diameter was measured using ImageJ). 10% Methacrylated hyaluronic acid (MeHA) was used as a control group.

2.8. Printability test

In this study, an Allevi 2 (Allevi) bioprinter was used to perform all the printing processes. After mixing with DTT, the bioink formulations were immediately transferred to a 10-mL syringe, and the syringe was mounted on the printer. To test the printability, the bioink was used to print a 15 mm × 15 mm grid-like 2-layer scaffold on a methacrylated glass slide (following the surface treatment protocol described previously [77]). The elapsed time was also recorded after mixing DTT in bioink formulation. Printing parameters were optimized with respect to this elapsed time to print uniform grids. Methacrylated hyaluronic acid (MeHA) was used as a control group. To print thick hydrogel scaffolds (>3 mm), 30% Pluronic F-127 was used as a support ink. After cross-linking process, the scaffolds were immersed in DPBS at 4 °C to remove Pluronic support. To print multi-material scaffolds, cCMC 1:4 and NorCMC 1:2 were prepared as mentioned. To distinguish different inks, 100 μl of food color was added to cCMC 1:4.

2.9. 3D bioprinting of cell-laden hydrogels

Cell-laden bioink (15%cCMC or 10%NorCMC) was printed on methacrylated glass slides at optimized parameters obtained from printability tests. The printed cell-laden scaffolds were immediately transferred into non-treated 6-well plates and 5 mL of growth media was added into each well. Methacrylated hyaluronic acid (MeHA) was used as a control group.

2.10. Cell viability tests

Cell-laden hydrogels were cultured for 7 days, and live-dead staining was performed at day 1, 4, and 7 to characterize the viability of the encapsulated cells. Cell-laden hydrogels were washed with DPBS and then stained with calcein-AM ("live", 0.5 μL/mL) and ethidium homodimer ("dead", 2 μL/mL) for 15 min. Samples were washed with DPBS and transferred to confocal laser scanning microscope (confocal and 2-photon scanning microscope, Leica) to capture fluorescent images of the cells. Two samples per group was prepared for each time point, and 3 random regions of the gel were scanned. The viability was calculated by counting cells using ImageJ.

2.11. Statistical methods

If not stated specifically we used three samples per each group for all studies. The data were analyzed using KaleidaGraph. Data are presented as mean ± standard deviation. ANOVA with Tukeys HSD post hoc test of means was used to make comparisons between sample groups.

3. Results

3.1. Bioink formulations

In this study, two distinct bioink formulations were developed from norbornene functionalized CMC (Fig. 1), either with an amide, NorCMC, or an ester linker, cCMC. ^{1}H NMR results confirmed 30% and 20% functionalization for cCMC and NorCMC, respectively (Supplementary Fig. S1). The compositions of the bioink formulations are given in Table 1. Bioinks were formulated at 15% cCMC and 10% NorCMC, with thiol to norbornene ratio (T:NB) equal to (1:4), (1:2), and (1:1).

3.2. Rheological test results

The initial shear viscosities of the bioink formulations were in the range of 0.8–2.8 Pa•s (Table 1). The gelation behavior of the

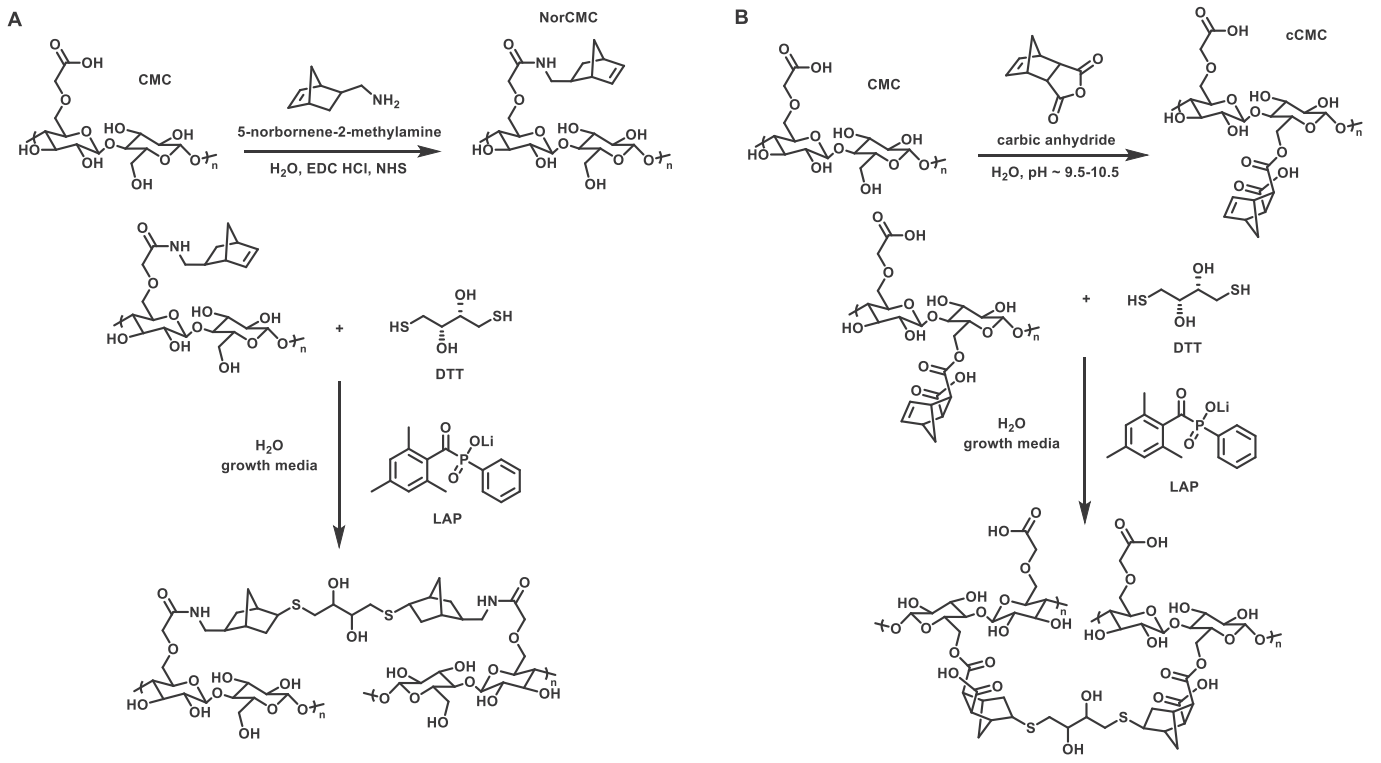

Fig. 1. Chemical structure, modification reaction, and crosslink mechanism of NorCMC (A) and cCMC (B).

Table 1
Composition, corresponding viscosities, and autogelation time of tested ink formulations.

Ink formulation	Polymer concentration	(T:NB)	Initial viscosity (Pa•s)	Gelation time (min)
cCMC (1:4)	15%	(1:4)	0.8 ± 0.10	91
cCMC (1:2)	15%	(1:2)	1.2 ± 0.10	57
cCMC (1:1)	15%	(1:1)	1.5 ± 0.03	29
NorCMC (1:4)	10%	(1:4)	0.8 ± 0.09	>180
NorCMC (1:2)	10%	(1:2)	1.2 ± 0.09	49
NorCMC (1:1)	10%	(1:1)	2.8 ± 0.03	26

formulations were characterized with time sweep experiments, in which the elastic modulus (G′), viscous modulus (G″), and phase angle (Φ) values were recorded (Fig. 2). For all of the formulations, autogelation behavior is observed within 3 h in the absence of UV light. The gel point, i.e., onset of gelation, and the elapsed time for equilibrium for each formulation are summarized in Table 1. The gel point decreased with increasing T:NB, or increasing crosslinker concentration. For cCMC, gelation time significantly increased from 29 min (1:1) to 91 min (1:4). For NorCMC, gelation time values were 26, 40, and greater than 180 min, for (1:1), (1:2), and (1:4), respectively.

To investigate the gelation under light exposure, samples were exposed to UV light during time sweep tests (Fig. 3, Supplementary Fig. S2). For cCMC, independent from T:NB, gel point was equal to ~18 s, and it took approximately 120 s for crosslinking reaction to reach equilibrium. For NorCMC, the gelation time and equilibrium time were equal to ~5 s and ~60 s, respectively. The magnitude of the equilibrium shear modulus (G') was determined by the composition of the ink formulation, such that a higher (T:NB) resulted in a higher G'. For cCMC formulations, the equilibrium values for G' were equal to ~3200 Pa for (1:4) and ~9300 Pa for (1:2). For NorCMC, the equilibrium values for G' were equal to ~4600 Pa for (1:4) and ~8700 Pa for (1:2).

3.3. Mechanical tests results

To probe the mechanical properties, the compression moduli were measured using 3D printed samples from all of the ink formulations. As shown in Fig. 4, for the same macromers, higher (T:NB) resulted in higher compressive moduli. For 15% cCMC, the compressive modulus increased by ~7-fold (from 46 to 316 kPa) when the (T:NB) increased from (1:4) to (1:2). The same trend was observed for 10% NorCMC, but the increment was less than 3.3-fold (from 40 to 133 kPa).

3.4. Swelling tests results

Swelling tests were conducted on 3D printed samples (Fig. 4B). Our results showed that increasing (T:NB) resulted in a 1.8 fold decrease in the swelling ratio (from 26 to 14) for cCMC, and a 1.6 fold decrease in the swelling ratio (from 24 to 15) for NorCMC.

3.5. Line test results

Fig. 5 shows the line test results for 15% cCMC and 10% NorCMC. MeHA (10%) was used as a control group. In general, strut size increased with increasing print pressure and decreasing print speed. For instance, at 10 mm/s, the line width increased from 920 to 1390 μm for cCMC, from 850 to 1790 μm for NorCMC, and from 1110 to 1720 μm for MeHA, when the pressure was increased from 138 kPa (20 psi) to 276 kPa (40 psi). When printed at 20 mm/s and 138 kPa print pressure, it was possible to achieve 630 μm for cCMC, 620 μm for cCMC, and 800 μm for MeHA.

3.6. Printability test results

Ink formulations from cCMC and NorCMC (both formulations with (T:NB) equal to (1:4) and (1:2)), were used to print grid-like scaffolds (Fig. 5) to investigate printability. The pressure was set at 138 kPa (20 psi) at the beginning (for 30 min delay time) and gradually increased to 276 kPa (40 psi, for 60 min delay time) and 345 kPa for (50psi, for 90 min delay time) to compensate the increment of the ink viscosity due to

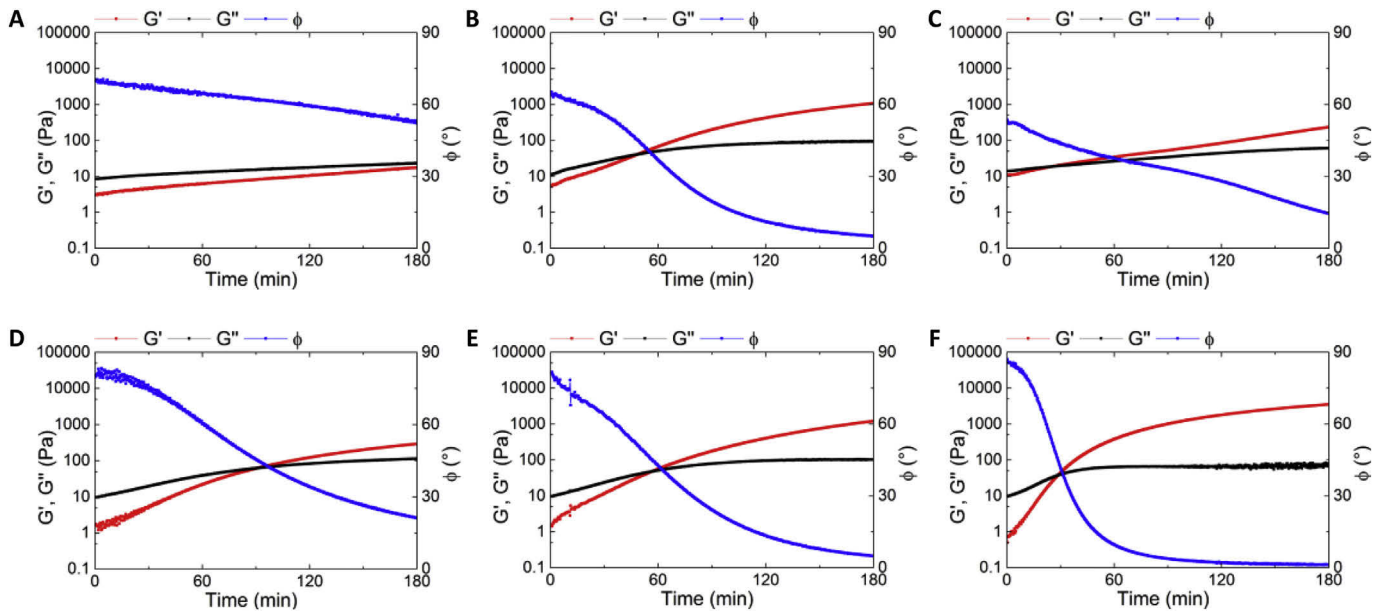

Fig. 2. Time sweep test of ink formulations without light exposure. (A-C) 10% NorCMC with thiol to norbornene ratio, (T:NB) equal to (1:4) (A), (1:2) (B), and 1:1 (C). (D-F) 15% cCMC with (T:NB) = 1:4 (D), 1:2 (E), and 1:1 (F).

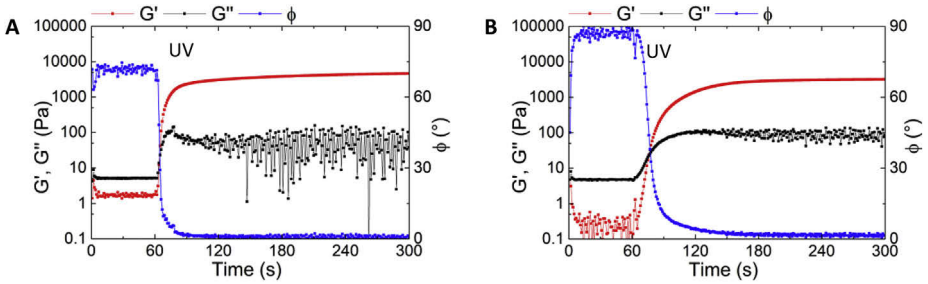

Fig. 3. Time sweep test of ink formulations under light exposure for: (A) NorCMC (1:4) and (B) cCMC (1:4). Green area denotes the UV exposure period. (For interpretation of the references to color in this figure legend, the reader is referred to the Web version of this article.)

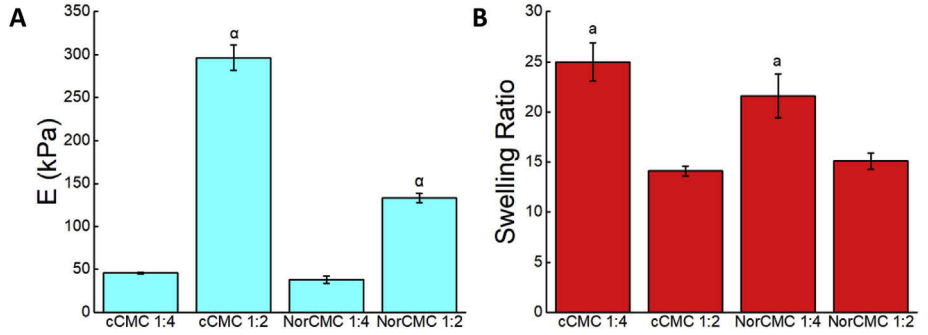

Fig. 4. (A) Compressive modulus (*E*) values of the 3D printed hydrogels from bioink formulations. $^{\alpha}p<0.005$ for cCMC (1:2), as compared to the rest of the sample groups, and for NorCMC (1:2), as compared to the other groups. (B) The equilibrium swelling ratios values of the 3D printed hydrogels. $^{a}p<0.005$ for cCMC (1:4) and for NorCMC (1:2), as compared to cCMC (1:2) and NorCMC (1:2).

autogelation. The print speed was controlled between 5 mm/s and 10 mm/s to print the gel with a uniform shape. Due to autogelation, ink formulations were not extrudable after a certain time for each formulation that was marked with a cross sign in Fig. 5. Dual material printing was used to bioprint thick hydrogel scaffolds (NorCMC (1:2)) supported with sacrificial Pluronic, and NorCMC (1:2) scaffolds with fast degrading cCMC (1:4) patterns (Fig. 6).

3.7. Bioprinting test results

Fig. 7A shows the cell viability data (in percentage) for hMSCs, 3T3 cells, and HUVECs. Note that cCMC sample group degraded in the medium after day 4. Fig. 7B shows the confocal images of the stained cells, in which the green indicates live cells and the red indicates dead cells. In the side view images, the range of cells in the vertical direction was different due to the different swelling properties for each ink formulation.

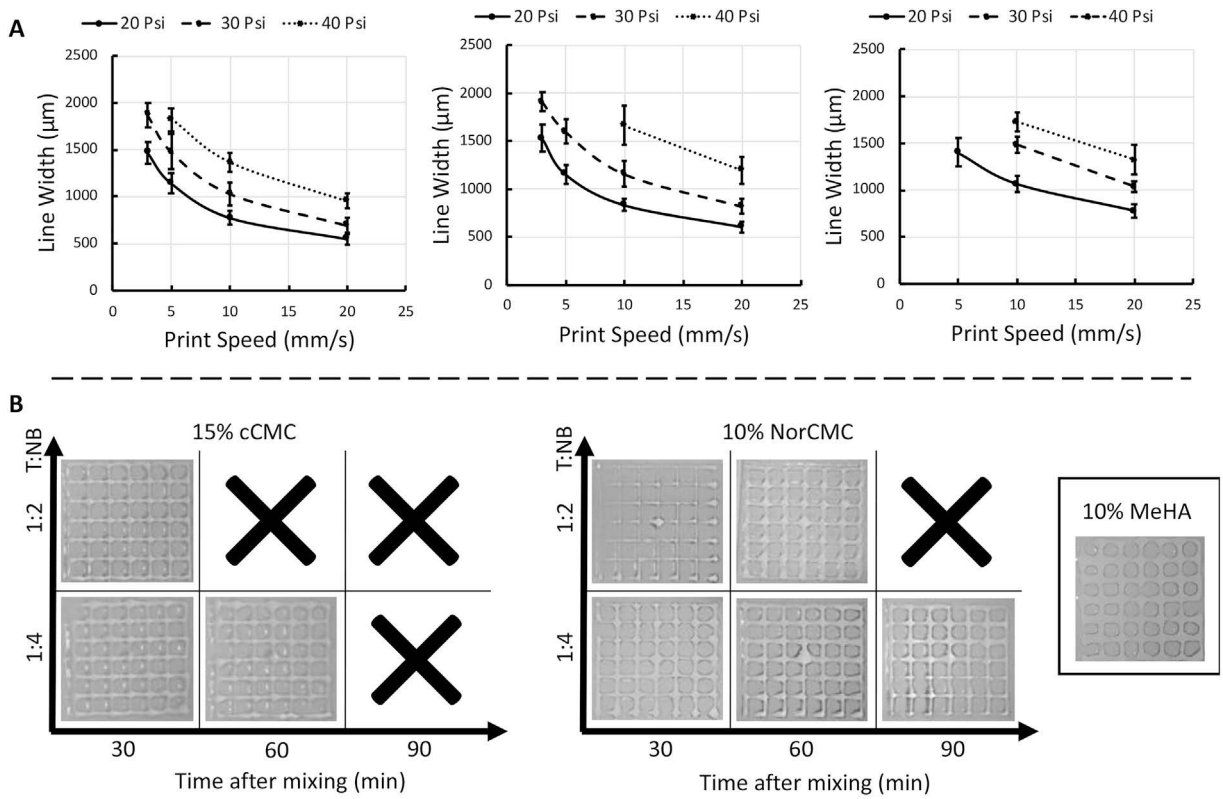

Fig. 5. (A) Line test results for 15% cCMC, 10% NorCMC and 10% MeHA bioinks. Error bars denote standard deviation for n ≥ 5. (B) Printability tests for 15% cCMC and 10% NorCMC for different (T:NB). The x-axis shows the elapsed time after mixing the crosslinker (DTT) with the ink formulation. Printability test result for 10% MeHA is given as a control.

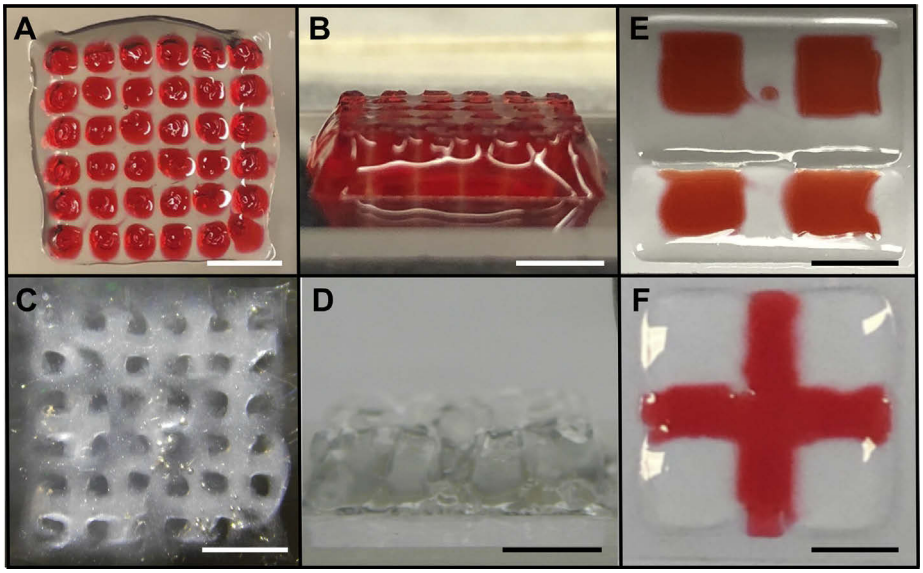

Fig. 6. Pictures showing multi-material printing of thick (>3 mm in height) scaffolds. (A-B) Top (A) and side (B) views of NorCMC (1:2) scaffold printed with Pluronic (red). (C-D) Scaffold after Pluronic is dissolved in PBS. (E-F) NorCMC (1:2) scaffolds printed with fast degrading cCMC (1:4) (red). Scale bars are 5 mm. (For interpretation of the references to color in this figure legend, the reader is referred to the Web version of this article.)

4. Discussion

Here, we report novel bioink formulations from norbornene modified, cellulose-based macromers for the first time. Cellulose-based materials are promising candidates as bioinks due to their inherent bioactivity, abundance and low cost. In this study, two distinct macromers were developed by functionalizing CMC with an amide (NorCMC) or an ester linker (cCMC) with 30% and 20% functionalization for cCMC and NorCMC, respectively. These degrees of functionalization were selected because hydrogels at the same thiol to norbornene ratio and low solids content (4 wt% polymer) yielded similar compression modulus values [74,75]. Our previous studies (utilizing the same extrusion-based printer) revealed that an initial viscosity in a range of 1–10 Pa•s was ideal for a non-shear-thinning hydrogel when a 27-gauge needle was

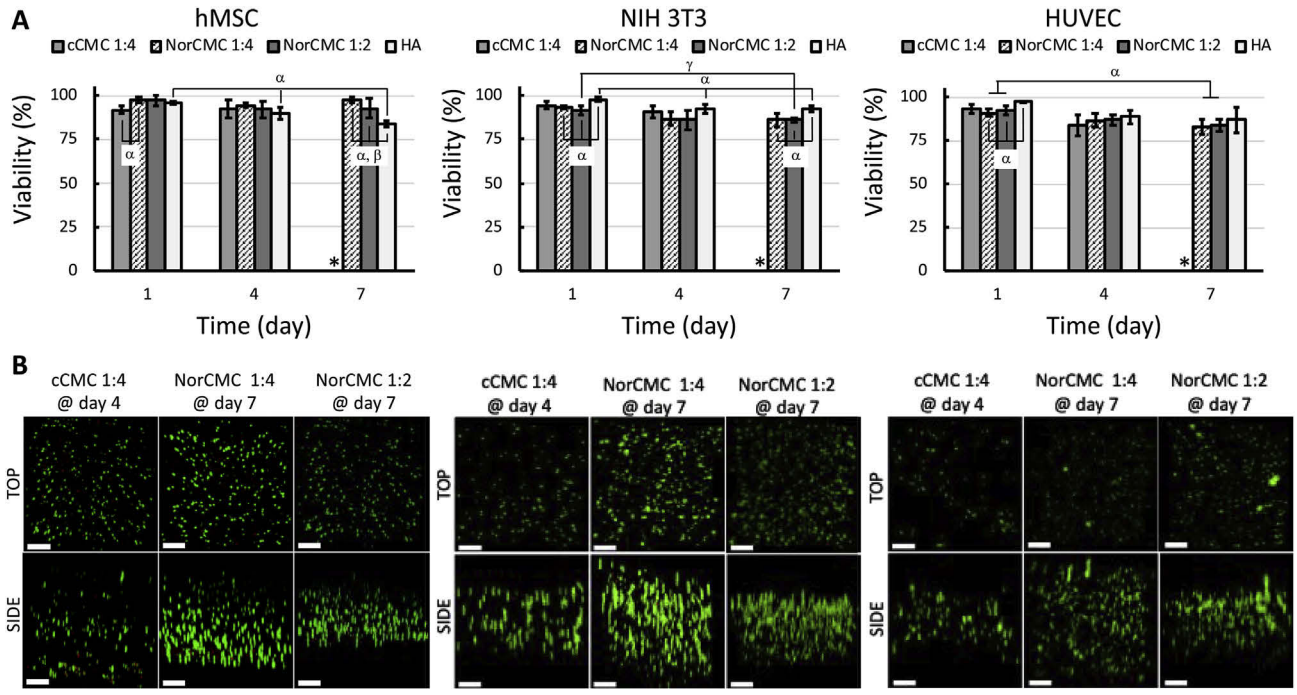

Fig. 7. (A) Plots showing % cell viability with culture time for cells (hMSCs, NIH 3T3 cells and HUVECs) cultured within bioprinted cCMC, NorCMC and MeHA hydrogels. * indicates the cCMC (1:4) sample group that degraded before day 7. (B) Confocal fluorescent images of cells (hMSCs, NIH 3T3 cells and HUVECs) within bioprinted cCMC, NorCMC and MeHA hydrogels (green indicating live cells and red indicating dead cells). (Scale bars are 200 μm) For hMSC, $^{\alpha}$ $p < 0.005$ cell viability for MeHA at day 1 vs. at day 4 and at day 7, and at day 4 vs. at day 7.; cell viability for cCMC (1:4) as compared to NorCMC (1:4) at day 1; cell viability for NorCMC (1:2) as compared to MeHA at day 7; $^{\beta}$ $p < 0.0001$ NorCMC (1:4) vs. MeHA at day 7. For NIH 3T3 cell line, $^{\alpha}$ $p < 0.005$ cell viability for MeHA at day 1 vs. day 4 and day 7; cell viability of MeHA as compared to NorCMC (1:2) and (1:4) ay day 1 and at day 7; $^{\gamma}$ p 0.005 $\leq$ for NorCMC at day 1 vs. day 7. For HUVECs, $^{\alpha}$ $p < 0.005$ cell viability for NorCMC (1:4) and (1:2) at day 1 vs. day 7; cell viability for MeHA as compared to NorCMC (1:2) and (1:4) at day 1. For all groups $n = 6$. (For interpretation of the references to color in this figure legend, the reader is referred to the Web version of this article.)

used [33]. To adjust the viscosity of the inks within this range, polymer concentrations were set to 15% for cCMC and 10% for NorCMC, due to differences in solubilities of the macromers. A higher concentration of cCMC was used as compared to NorCMC to yield similar bioink initial viscosities. The cCMC polymer is significantly easier to dissolve than NorCMC because additional carboxylic acid groups are introduced through the functionalization reaction (Fig. 1). This behavior translated into similar bioink viscosities at different polymer concentrations. Additionally, since the norbornenes are connected to the CMC with different functional groups, degradation behavior was expected to be different with the ester linkages of cCMC degrading earlier than the amides of NorCMC.

Crosslinker, or thiol, to norbornene ratio (T:NB) was systematically increased, from (1:4), (1:2) and to (1:1), to investigate the effect of (T:NB) on bioink properties. For cCMC, the viscosity values did not change significantly with (T:NB). However, for NorCMC, we observe a significant increase in viscosity with increasing (T:NB), such that a 2-fold increase in viscosity is observed when (T:NB) increased from (1:4) (0.8 Pa s) to (1:1) (2.8 Pa s). This we believe is due to the spontaneous crosslinking of the macromers in the absence of UV light, i.e., autogelation process. Rheological evaluation of the formulations revealed autogelation in all formulations, but the gel point (onset of gelation) decreased significantly with increasing (T:NB). The mechanism of this phenomena has not been understood yet, but it is previously reported that the autogelation accelerates with increasing thiol and norbornene concentrations, increasing temperature, dissolved oxygen, and acidic conditions [50]. Previous chemical characterization of the autogelation has indicated that it is still a thiol-norbornene reaction, which must be initiated through radicals spontaneously produced in the solution [50]. Future work aims to understand the origin of these radicals. Note that cCMC is acidic when directly dissolved in the growth media or PBS (pH reaching to ~4) due to the presence of carboxylic acid units in the carbic groups. Therefore, we adjusted the pH to 7.6 (as described in the experimental section) to mainly eliminate cell viability issues. We found that cCMC could form a gel within few minutes when the pH is not adjusted **(**Supplementary Fig. S3**)**. Considering the autogelation behavior of our macromers, the gelation time (gel point) is considered as a critical parameter for planning the printing process, since these hydrogels were not extrudable when gelled. Considering the time required for pre-printing process, we decided to eliminate the macromer formulations with gel point below 1 h (Table 1 and Fig. 5). Thus, macromer formulations with highest (T:NB), (1:1), for both macromers were eliminated.

Norbornene groups allowed the macromers to be photoresponsive which can lead to crosslinking in the presence of a photoinitiator (LAP) and a crosslinker (DTT) when exposed to light. Rheological tests in the presence of a UV light source allowed us to determine the photocrosslinking parameters to be used during the bioprinting process. For cCMC, it required ~18 s to gel and ~120 s to completely crosslink, which directed us to set the partial crosslink time to be 30 s and the post-print crosslinking time to be 120 s (Fig. 3). The crosslink setting for NorCMC was also set as 10 s for partial crosslinking and 90s for post-print crosslinking. The printability tests were conducted to evaluate the printability and to optimize the print parameters (print speed, print pressure, layer height, blue light exposure time). In the printing phase, some deviations between the rheological data (Fig. 2) and printing results (Fig. 5) were observed. In Fig. 2E, the gelation time of cCMC 1:2 was 57 min, which means that the available time for printing should be around 1 h. However, as shown in Fig. 5, cCMC 1:2 was not printable after 30 min. We believe that this is caused by the undermixing of the gel solution and the crosslinker leading to localized gelation in the syringe due to increased thiol concentration. Vigorous mixing such as vortex is not suitable for viscous ink formulations, and ink can gel during gentle, but longer, mixing process. Due to these concerns, cCMC 1:2 was eliminated from further study.

Our results indicate that the thiol to norbornene ratio (T:NB) of the bioink formulation, controlled by the crosslinker concentration, also affects the mechanical properties of the hydrogel (Fig. 4A). Normally, at the molecular level, increasing crosslinker concentration leads to an increase in the compressive modulus (Young's modulus, *E*). Thus, as expected the *E* values increased significantly with increase in (T:NB) from (1:4) to (1:2) for both cCMC and NorCMC.

For each bioink formulation, we compared the cell viability with culture time for each cell line. For instance, hMSC viability decreased from 96% at day 1–90% at day 4, and to 84% at day 7 for MeHA control group. Note that MeHA is not degradable, and this could potentially eliminate the ability of the hMSCs to spread and proliferate. However, hMSC viability was not significantly different for other degradable formulations, such that cell viability remained stable within 92–93% interval for cCMC (1:4), 95–97% interval for NorCMC (1:4), and 97-93% interval for NorCMC (1:2). When NIH 3T3 cells are considered, cell viability decreased for NorCMC (1:2) from 92% at day 1–83% at day 7, and for MeHA from 97% at day 1, to 88% at day 4, and to 87% at day 7. Cell viability did not show a significant change, and remained constant within 93-83% for cCMC (1:4) and within 91%–83% for NorCMC (1:4). For HUVECs, cell viability decreased from 93% at day 1–86% at day 7 for NorCMC (1:4) and from 91% at day 1–86% at day 7, whereas the changes were not significant between day 1 and day 4 (including cCMC group), and day 4 and day 7. Cell viability for MeHA group remained within 97-93%. Our results showed that the decrease in cell viability for the NorCMC and cCMC formulations is not trivial, and dependent on the cell type and culture period. As we did not use any commonly used cell-adhesive peptides (such as RGD), we believe that cell variability could potentially be further enhanced, if needed. We also compared the cell viability between sample groups (bioink formulations) for each cell line at each culture day. For hMSCs, cell viability for cCMC (92%) was lower than that for NorCMC (1:4) (97%) at day 1. No significant difference was observed between sample groups at day 4. However, cell viability for MeHA (84%) was lower than that for NorCMC (1:2) (93%) and for NorCMC (1:4) (97%) at day 7. For 3T3 cell line, cell viability for MeHA (97% at day 1, 87% at day 7) was higher than that for NorCMC (1:2) (92% at day 1, 83% at day 7) and NorCMC (1:4) (91% at day 1, 83% at day 7) at day 1 and day 7. When HUVECs are considered, cell viability for MeHA (98%) was higher than cell viability for NorCMC (1:2) (91%) and NorCMC (1:4) (93%) at day 1. No significant difference was observed between sample groups at day 4 and day 7. We believe that a lower cell viability at day 1 could potentially indicate issues during printing process, such as cell damage due to shear or light exposure. One way to avoid this is to increase the bioink viscosity to protect the cells. For instance, MeHA bioinks were much viscous leading to higher cell viability at day 1.

The 15% cCMC (1:4) sample degraded and disintegrated by day-7 while the similar NorCMC (1:4) did not because of the reduced degradation afforded by the amide connectivity versus the ester groups connecting the norbornenes to the CMC. Hydrolytic degradation of the cCMC bulk hydrogels was previously reported, such that for 4% cCMC with (T:NB) equal to (1:4), 30% mass loss was reported within 24 h incubation, which increased to ~50% after 7days [74]. This behavior was not observed for NorCMC hydrogels [75]. In good agreement with the swelling data (see above), we observed differences in the confocal side view images (Fig. 7B) of the 3D printed samples. For instance, vertical distribution of the cells within NorCMC (1:4) was about twice thicker than NorCMC (1:2), which corresponded to the difference in the swelling ratio (23.4 for NorCMC (1:4), 12 for NorCMC (1:2)). For cCMC (1:4), cells distributed more sparsely when compared to that for NorCMC. We believe that this was due to hydrogel degradation as discussed above.

5. Conclusions

In conclusion, we report a two norbornene-modified cellulose-based macromers as novel bioink materials. Polymer concentration and thiol:norbornene ratio (T:NB) were optimized to prepare printable bioink formulations from cCMC (with (T:NB) = (1:2) and (1:4)) and NorCMC (with (T:NB) = (1:4)). All of the ink formulations were able to encapsulate cells (hMSCs, NIH 3T3 fibroblasts, and HUVECs), and to be printed as cell-laden scaffolds. We believe that these two cellulose-based macromers broaden the bioink library and could be further modified to render more desired properties in further practice and applications.

Declaration of competing interest

The authors declare that they have no known competing financial interests or personal relationships that could have appeared to influence the work reported in this paper.

CRediT authorship contribution statement

Shen Ji: Writing - original draft, Formal analysis, Data curation. **Alperen Abaci:** Formal analysis. **Tessali Morrison:** Formal analysis. **William M. Gramlich:** Supervision, Writing - review & editing. **Murat Guvendiren:** Supervision, Writing - review & editing, Data curation, Formal analysis.

Acknowledgements

This work is partially funded by the National Science Foundation Award Number DMR-1714882 (M.G.), and by the Faculty Seed Grant (M.G.) from the Center for Engineering MechanoBiology (CEMB), an NSF Science and Technology Center, under grant agreement CMMI: 15-48571. Use of the Bruker Avance NEO 500MHz nuclear magnetic resonance (NMR) spectrometer was supported by the National Science Foundation under grant CHE-1828408. Any opinions, findings, and conclusions or recommendations expressed in this material are those of the authors and do not necessarily reflect the views of the National Science Foundation.

Appendix A. Supplementary data

Supplementary data to this article can be found online at https://doi.org/10.1016/j.bprint.2020.e00083.

References

[1] L. Archer, 3D printing with living inks, Science 358 (6367) (2017) 1143.
[2] H. Cui, M. Nowicki, J.P. Fisher, L.G. Zhang, 3D bioprinting for organ regeneration, Adv. Healthc. Mater. 2017 (6) (2016), 1601118.
[3] A.B. Dababneh, I.T. Ozbolat, Bioprinting technology: a current State-of-the-Art review, J. Manuf. Sci. Eng. 136 (6) (2014), 061016.
[4] S.V. Murphy, A. Atala, 3D bioprinting of tissues and organs, Nat. Biotechnol. 32 (8) (2014) 773–785.
[5] H.W. Kang, S.J. Lee, I.K. Ko, C. Kengla, J.J. Yoo, A. Atala, A 3D bioprinting system to produce human-scale tissue constructs with structural integrity, Nat. Biotechnol. 34 (3) (2016) 312–319.
[6] B. Grigoryan, S.J. Paulsen, D.C. Corbett, D.W. Sazer, C.L. Fortin, A.J. Zaita, P.T. Greenfield, N.J. Calafat, J.P. Gounley, A.H. Ta, F. Johansson, A. Randles, J.E. Rosenkrantz, J.D. Louis-Rosenberg, P.A. Galie, K.R. Stevens, J.S. Miller, Multivascular networks and functional intravascular topologies within biocompatible hydrogels, Science 364 (6439) (2019) 458.
[7] N. Noor, A. Shapira, R. Edri, I. Gal, L. Wertheim, T. Dvir, 3D Printing of personalized thick and perfusable cardiac patches and hearts, Adv. Sci. 6 (11) (2019) 1900344.
[8] V. Mironov, V. Kasyanov, R.R. Markwald, Organ printing: from bioprinter to organ biofabrication line, Curr. Opin. Biotechnol. 22 (5) (2011) 667–673.
[9] C.Y. Liaw, M. Guvendiren, Current and emerging applications of 3D printing in medicine, Biofabrication 9 (2) (2017), 024102.
[10] C.-Y. Liaw, S. Ji, M. Guvendiren, Engineering 3D hydrogels for personalized in vitro human tissue models, Adv. Healthc. Mater. 7 (4) (2018) 1701165.
[11] X. Ma, J. Liu, W. Zhu, M. Tang, N. Lawrence, C. Yu, M. Gou, S. Chen, 3D bioprinting of functional tissue models for personalized drug screening and in vitro disease modeling, Adv. Drug Deliv. Rev. 132 (2018) 235–251.
[12] J. Jang, H.-G. Yi, D.-W. Cho, 3D Printed tissue models: present and future, ACS Biomater. Sci. Eng. 2 (10) (2016) 1722–1731.
[13] L.M. Norona, D.G. Nguyen, D.A. Gerber, S.C. Presnell, M. Mosedale, P.B. Watkins, Bioprinted liver provides early insight into the role of Kupffer cells in TGF-β1 and methotrexate-induced fibrogenesis, PloS One 14 (1) (2019), e0208958.

[14] M. Albanna, K.W. Binder, S.V. Murphy, J. Kim, S.A. Qasem, W. Zhao, J. Tan, I.B. El-Amin, D.D. Dice, J. Marco, J. Green, T. Xu, A. Skardal, J.H. Holmes, J.D. Jackson, A. Atala, J.J. Yoo, In situ bioprinting of autologous skin cells accelerates wound healing of extensive excisional full-thickness wounds, Sci. Rep. 9 (1) (2019) 1856.
[15] N. Ashammakhi, S. Ahadian, I. Pountos, S.-K. Hu, N. Tellisi, P. Bandaru, S. Ostrovidov, M.R. Dokmeci, A. Khademhosseini, In situ three-dimensional printing for reparative and regenerative therapy, Biomed. Microdevices 21 (2) (2019) 42.
[16] V. Keriquel, H. Oliveira, M. Rémy, S. Ziane, S. Delmond, B. Rousseau, S. Rey, S. Catros, J. Amédée, F. Guillemot, J.-C. Fricain, In situ printing of mesenchymal stromal cells, by laser-assisted bioprinting, for in vivo bone regeneration applications, Sci. Rep. 7 (1) (2017) 1778.
[17] J. Groll, J.A. Burdick, D.W. Cho, B. Derby, M. Gelinsky, S.C. Heilshorn, T. Jungst, J. Malda, V.A. Mironov, K. Nakayama, A. Ovsianikov, W. Sun, S. Takeuchi, J.J. Yoo, T.B.F. Woodfield, A definition of bioinks and their distinction from biomaterial inks, Biofabrication 11 (1) (2018), 013001.
[18] T.I. Ozbolat, K.K. Moncal, H. Gudapati, Evaluation of bioprinter technologies, Addit. Manuf. (2016).
[19] H. Gudapati, M. Dey, I. Ozbolat, A comprehensive review on droplet-based bioprinting: past, present and future, Biomaterials 102 (2016) 20–42.
[20] A. Shafiee, A. Atala, Printing technologies for medical applications, Trends Mol. Med. 22 (3) (2016) 254–265.
[21] S. Ji, M. Guvendiren, Recent advances in bioink design for 3D bioprinting of tissues and organs, Front. Bioeng. Biotechnol. 5 (2017) 23.
[22] K. Dubbin, A. Tabet, S.C. Heilshorn, Quantitative criteria to benchmark new and existing bio-inks for cell compatibility, Biofabrication 9 (4) (2017), 044102.
[23] K. Holzl, S. Lin, L. Tytgat, S. Van Vlierberghe, L. Gu, A. Ovsianikov, Bioink properties before, during and after 3D bioprinting, Biofabrication 8 (3) (2016), 032002.
[24] D. Chimene, K.K. Lennox, R.R. Kaunas, A.K. Gaharwar, Advanced bioinks for 3D printing: a materials science perspective, Ann. Biomed. Eng. 44 (6) (2016) 2090–2102.
[25] P.S. Gungor-Ozkerim, I. Inci, Y.S. Zhang, A. Khademhosseini, M.R. Dokmeci, Bioinks for 3D bioprinting: an overview, Biomater. Sci. 6 (5) (2018) 915–946.
[26] M. Hospodiuk, M. Dey, D. Sosnoski, I.T. Ozbolat, The bioink: a comprehensive review on bioprintable materials, Biotechnol. Adv. 35 (2) (2017) 217–239.
[27] D.B. Kolesky, K.A. Homan, M.A. Skylar-Scott, J.A. Lewis, Three-dimensional bioprinting of thick vascularized tissues, Proc. Natl. Acad. Sci. Unit. States Am. 113 (12) (2016) 3179.
[28] D.B. Kolesky, R.L. Truby, A.S. Gladman, T.A. Busbee, K.A. Homan, J.A. Lewis, 3D bioprinting of vascularized, heterogeneous cell-laden tissue constructs, Adv. Mater. 26 (19) (2014) 3124–3130.
[29] A.L. Rutz, K.E. Hyland, A.E. Jakus, W.R. Burghardt, R.N. Shah, A multimaterial bioink method for 3D printing tunable, cell-compatible hydrogels, Adv. Mater. 27 (9) (2015) 1607–1614.
[30] C. Colosi, S.R. Shin, V. Manoharan, S. Massa, M. Costantini, A. Barbetta, M.R. Dokmeci, M. Dentini, A. Khademhosseini, Microfluidic bioprinting of heterogeneous 3D tissue constructs using low-viscosity bioink, Adv. Mater. 28 (4) (2016) 677–684.
[31] K.S. Lim, B.S. Schon, N.V. Mekhileri, G.C.J. Brown, C.M. Chia, S. Prabakar, G.J. Hooper, T.B.F. Woodfield, New visible-light photoinitiating system for improved print fidelity in gelatin-based bioinks, ACS Biomater. Sci. Eng. 2 (10) (2016) 1752–1762.
[32] J. Yin, M. Yan, Y. Wang, J. Fu, H. Suo, 3D bioprinting of low-concentration cell-laden gelatin methacrylate (GelMA) bioinks with a two-step cross-linking strategy, ACS Appl. Mater. Interfaces 10 (8) (2018) 6849–6857.
[33] S. Ji, E. Almeida, M. Guvendiren, 3D bioprinting of complex channels within cell-laden hydrogels, Acta Biomater. 95 (2019) 214–224.
[34] C.B. Highley, C.B. Rodell, J.A. Burdick, Direct 3D printing of shear-thinning hydrogels into self-healing hydrogels, Adv. Mater. 27 (34) (2015) 5075–5079.
[35] S. Khalil, W. Sun, Bioprinting endothelial cells with alginate for 3D tissue constructs, J. Biomech. Eng. 131 (11) (2009).
[36] H. Yi, L.-Q. Wu, W.E. Bentley, R. Ghodssi, G.W. Rubloff, J.N. Culver, G.F. Payne, Biofabrication with chitosan, Biomacromolecules 6 (6) (2005) 2881–2894.
[37] K.K. Moncal, V. Ozbolat, P. Datta, D.N. Heo, I.T. Ozbolat, Thermally-controlled extrusion-based bioprinting of collagen, J. Mater. Sci. Mater. Med. 30 (5) (2019) 55.
[38] S. Rhee, J.L. Puetzer, B.N. Mason, C.A. Reinhart-King, L.J. Bonassar, 3D bioprinting of spatially heterogeneous collagen constructs for cartilage tissue engineering, ACS Biomater. Sci. Eng. 2 (10) (2016) 1800–1805.
[39] C. Lee, E. Abelseth, L. de la Vega, S.M. Willerth, Bioprinting a novel glioblastoma tumor model using a fibrin-based bioink for drug screening, Mater. Today Chem. 12 (2019) 78–84.
[40] Z. Zheng, J. Wu, M. Liu, H. Wang, C. Li, M.J. Rodriguez, G. Li, X. Wang, D.L. Kaplan, 3D bioprinting of self-standing silk-based bioink, Adv. Healthc. Mater. 7 (6) (2018) 1701026.
[41] S. Chawla, S. Midha, A. Sharma, S. Ghosh, Silk-based bioinks for 3D bioprinting, Adv. Healthc. Mater. 7 (8) (2018) 1701204.
[42] J. Jang, T.G. Kim, B.S. Kim, S.-W. Kim, S.-M. Kwon, D.-W. Cho, Tailoring mechanical properties of decellularized extracellular matrix bioink by vitamin B2-induced photo-crosslinking, Acta Biomater. 33 (2016) 88–95.
[43] J. Jang, H.-J. Park, S.-W. Kim, H. Kim, J.Y. Park, S.J. Na, H.J. Kim, M.N. Park, S.H. Choi, S.H. Park, S.W. Kim, S.-M. Kwon, P.-J. Kim, D.-W. Cho, 3D printed complex tissue construct using stem cell-laden decellularized extracellular matrix bioinks for cardiac repair, Biomaterials 112 (2017) 264–274.
[44] M. Kesti, M. Muller, J. Becher, M. Schnabelrauch, M. D'Este, D. Eglin, M. Zenobi-Wong, A versatile bioink for three-dimensional printing of cellular scaffolds based on thermally and photo-triggered tandem gelation, Acta Biomater. 11 (2015) 162–172.
[45] L.E. Bertassoni, C.J. C, V. Manoharan, A.L. Cristino, N.S. Bhise, W.A. Araujo, P. Zorlutuna, N.E. Vrana, A.M. Ghaemmaghami, M.R. Dokmeci, A. Khademhosseini, Direct-write bioprinting of cell-laden methacrylated gelatin hydrogels, Biofabrication 6 (2) (2014), 024105.
[46] W. Liu, M.A. Heinrich, Y. Zhou, A. Akpek, N. Hu, X. Liu, X. Guan, Z. Zhong, X. Jin, A. Khademhosseini, Y.S. Zhang, Extrusion bioprinting of shear-thinning gelatin methacryloyl bioinks, Adv. Healthc. Mater. 6 (12) (2017), https://doi.org/10.1002/adhm.201601451.
[47] J. Schurz, A bright future for cellulose, Prog. Polym. Sci. 24 (4) (1999) 481–483.
[48] C. Chang, L. Zhang, Cellulose-based hydrogels: present status and application prospects, Carbohydr. Polym. 84 (1) (2011) 40–53.
[49] D. Klemm, B. Heublein, H.P. Fink, A. Bohn, Cellulose: fascinating biopolymer and sustainable raw material, Angew Chem. Int. Ed. Engl. 44 (22) (2005) 3358–3393.
[50] T. McOscar, Renewable hydrogels from norbornene-functionalized carboxymethyl cellulose and a short dithiol crosslinked via a thiol-ene reaction, Electronic Theses and Dissertations 2761 (2017).
[51] A.S. Gladman, E.A. Matsumoto, R.G. Nuzzo, L. Mahadevan, J.A. Lewis, Biomimetic 4D printing, Nat. Mater. 15 (4) (2016) 413–418.
[52] Q. Wang, J. Sun, Q. Yao, C. Ji, J. Liu, Q. Zhu, 3D printing with cellulose materials, Cellulose 25 (8) (2018) 4275–4301.
[53] A. Cataldi, D. Rigotti, V.D.H. Nguyen, A. Pegoretti, Polyvinyl alcohol reinforced with crystalline nanocellulose for 3D printing application, Mater. Today Commun. 15 (2018) 236–244.
[54] L. Li, Y. Zhu, J. Yang, 3D bioprinting of cellulose with controlled porous structures from NMMO, Mater. Lett. 210 (2018) 136–138.
[55] H. Martínez Ávila, S. Schwarz, N. Rotter, P. Gatenholm, 3D bioprinting of human chondrocyte-laden nanocellulose hydrogels for patient-specific auricular cartilage regeneration, Bioprinting 1–2 (2016) 22–35.
[56] I. Henriksson, P. Gatenholm, D.A. Hägg, Increased lipid accumulation and adipogenic gene expression of adipocytes in 3D bioprinted nanocellulose scaffolds, Biofabrication 9 (1) (2017), 015022.
[57] K.M.O. Håkansson, I.C. Henriksson, C. de la Peña Vázquez, V. Kuzmenko, K. Markstedt, P. Enoksson, P. Gatenholm, Solidification of 3D printed nanofibril hydrogels into functional 3D cellulose structures, Adv. Mater. Technol. 1 (7) (2016) 1600096.
[58] M. Müller, E. Öztürk, Ø. Arlov, P. Gatenholm, M. Zenobi-Wong, Alginate sulfate–nanocellulose bioinks for cartilage bioprinting applications, Ann. Biomed. Eng. 45 (1) (2017) 210–223.
[59] D. Nguyen, D.A. Hägg, A. Forsman, J. Ekholm, P. Nimkingratana, C. Brantsing, T. Kalogeropoulos, S. Zaunz, S. Concaro, M. Brittberg, A. Lindahl, P. Gatenholm, A. Enejder, S. Simonsson, Cartilage tissue engineering by the 3D bioprinting of iPS cells in a nanocellulose/alginate bioink, Sci. Rep. 7 (1) (2017) 658.
[60] K. Schütz, A.-M. Placht, B. Paul, S. Brüggemeier, M. Gelinsky, A. Lode, Three-dimensional plotting of a cell-laden alginate/methylcellulose blend: towards biofabrication of tissue engineering constructs with clinically relevant dimensions, J. Tissue Eng. Regen. Med. 11 (5) (2017) 1574–1587.
[61] K. Markstedt, A. Mantas, I. Tournier, H. Martinez Avila, D. Hagg, P. Gatenholm, 3D bioprinting human chondrocytes with nanocellulose-alginate bioink for cartilage tissue engineering applications, Biomacromolecules 16 (5) (2015) 1489–1496.
[62] K. Markstedt, A. Escalante, G. Toriz, P. Gatenholm, Biomimetic inks based on cellulose nanofibrils and cross-linkable xylans for 3D printing, ACS Appl. Mater. Interfaces 9 (46) (2017) 40878–40886.
[63] N. Contessi Negrini, L. Bonetti, L. Contili, S. Farè, 3D printing of methylcellulose-based hydrogels, Bioprinting 10 (2018), e00024.
[64] H. Li, Y.J. Tan, K.F. Leong, L. Li, 3D bioprinting of highly thixotropic alginate/Methylcellulose hydrogel with strong interface bonding, ACS Appl. Mater. Interfaces 9 (23) (2017) 20086–20097.
[65] C.E. Hoyle, C.N. Bowman, Thiol-ene click chemistry, Angew Chem. Int. Ed. Engl. 49 (9) (2010) 1540–1573.
[66] S.K. Reddy, N.B. Cramer, C.N. Bowman, Thiol−Vinyl mechanisms. 2. Kinetic modeling of ternary Thiol−Vinyl photopolymerizations, Macromolecules 39 (10) (2006) 3681–3687.
[67] B.D. Fairbanks, M.P. Schwartz, A.E. Halevi, C.R. Nuttelman, C.N. Bowman, K.S. Anseth, A versatile synthetic extracellular matrix mimic via thiol-norbornene photopolymerization, Adv. Mater. 21 (48) (2009) 5005–5010.
[68] W.M. Gramlich, I.L. Kim, J.A. Burdick, Synthesis and orthogonal photopatterning of hyaluronic acid hydrogels with thiol-norbornene chemistry, Biomaterials 34 (38) (2013) 9803–9811.
[69] H.W. Ooi, C. Mota, A.T. Ten Cate, A. Calore, L. Moroni, M.B. Baker, Thiol-ene alginate hydrogels as versatile bioinks for bioprinting, Biomacromolecules 19 (8) (2018) 3390–3400.
[70] K.H. Song, C.B. Highley, A. Rouff, J.A. Burdick, Complex 3D-printed microchannels within cell-degradable hydrogels, Adv. Funct. Mater. 28 (31) (2018) 1801331.
[71] Z. Mũnoz, H. Shih, C.-C. Lin, Gelatin hydrogels formed by orthogonal thiol–norbornene photochemistry for cell encapsulation, Biomater. Sci. 2 (8) (2014) 1063–1072.
[72] H.D. Nguyen, H.-Y. Liu, B.N. Hudson, C.-C. Lin, Enzymatic cross-linking of dynamic thiol-norbornene click hydrogels, ACS Biomater. Sci. Eng. 5 (3) (2019) 1247–1256.
[73] Z. Jiang, R. Shaha, K. Jiang, R. McBride, C. Frick, J. Oakey, Composite hydrogels with controlled degradation in 3D printed scaffolds, IEEE Trans. NanoBioscience 18 (2) (2019) 261–264.
[74] T.V.C. McOscar, W.M. Gramlich, Hydrogels from norbornene-functionalized carboxymethyl cellulose using a UV-initiated thiol-ene click reaction, Cellulose 25 (11) (2018) 6531–6545.

[75] N. Dadoo, S.B. Landry, J.D. Bomar, W.M. Gramlich, Synthesis and spatiotemporal modification of biocompatible and stimuli-responsive carboxymethyl cellulose hydrogels using thiol-norbornene chemistry, Macromol. Biosci. 17 (9) (2017).
[76] B.D. Fairbanks, M.P. Schwartz, C.N. Bowman, K.S. Anseth, Photoinitiated polymerization of PEG-diacrylate with lithium phenyl-2,4,6-trimethylbenzoylphosphinate: polymerization rate and cytocompatibility, Biomaterials 30 (35) (2009) 6702–6707.
[77] M. Guvendiren, S. Yang, J.A. Burdick, Swelling-induced surface patterns in hydrogels with gradient crosslinking density, Adv. Funct. Mater. 19 (19) (2009) 3038–3045.